Available online at
https://mijuitm.com.my

e-ISSN: 2735-0703

Mathematical Sciences and Informatics Journal 7(2) 2026, 310–326

Mathematical Sciences and Informatics Journal

Optimal control analysis of preventive and treatment measures for cholera-typhoid co-infections

Abdu Masanawa Sagir[1], Chinenye Nworah[1*], Yusuf A. Bichi[1], Joel M. Orverem[1]

[1]*Department of Mathematics, Federal University Dutsin-Ma, Katsina State, Nigeria*

ARTICLE INFO

Article history:
Received 22 April 2026
Revised 2 June 2026
Accepted 18 June 2026
Online first
Published 5 October 2026

Keywords:
Cholera
Typhoid fever
Co-infection model
Optimal control
Basic reproduction number
Cost-effectiveness analysis

DOI:
10.24191/mij.v7i2.12400

ABSTRACT

Cholera and typhoid fever continue to threaten public health, particularly in communities with inadequate sanitation and unsafe water supplies. A compartmental framework is developed to investigate the joint spread of cholera and typhoid within a homogeneous population. The model accounts for direct and indirect transmission, environmental bacterial contamination, exposed and infectious classes, treatment, vaccination, recovery, and waning immunity. The next-generation matrix technique yielded the basic reproduction number R_0, which was used to determine the conditions for disease persistence. Mathematical analysis confirms that the model solutions remain positive and bounded at all times. Stability results indicate that the disease-free equilibrium is globally asymptotically stable whenever $R_0 < 1$, whereas endemic persistence is possible when $R_0 > 1$. To assess intervention measures, we introduced optimal control variables representing sanitation, vaccination, and treatment and analyzed them using Pontryagin's Maximum Principle. Numerical simulations demonstrate that combined interventions substantially reduce cholera prevalence, co-infection cases, and environmental bacterial concentrations. Sensitivity results indicate that cholera transmission is strongly influenced by environmental sanitation, whereas typhoid spread depends more on direct human contact. Cost-effectiveness analysis reveals that sanitation-focused interventions provide the most economical strategy for cholera control, whereas integrated measures achieve the largest overall reduction in disease burden.

1. INTRODUCTION

Cholera is a waterborne bacterial disease caused by *Vibrio cholerae*. Infection typically causes severe diarrhea and dehydration and is often linked to consuming contaminated water or food. The disease has an

[1*] Corresponding author. E-mail address: chinenyenworah2020@gmail.com

 ©Authors, 2026

estimated incubation period of 14 days (Azman et al., 2013). Typhoid fever, caused by *Salmonella enterica* serovar Typhi, is another life-threatening illness that shares transmission pathways with cholera (Akinyemi et al., 2021). It severely damages the reticuloendothelial system, intestinal lymphoid tissues, and the gallbladder, with an incubation period of about 3 to 19 days (Gouda, 2024).

Mathematical modeling has been central to understanding the dynamics of co-infections in human populations. For instance, reducing the basic reproduction number below unity has been shown to significantly lower malaria and pneumonia cases in a malaria–pneumonia co-infection model. Similarly, Sibaroni et al. (2020) highlighted that environmental and climatic variability can significantly influence the spread and endemicity of infectious diseases, including dengue fever, emphasizing the role of environmental forcing in disease propagation. Furthermore, an SIR framework was applied to analyze COVID-19 interventions in Malaysia, showing the effectiveness of mathematical models in evaluating public health control strategies.

Cholera and typhoid fever remain significant public health threats globally, particularly in regions with inadequate sanitation and water sources unsafe for human consumption (Ali et al., 2015; Stanaway et al., 2019). The disease burden is disproportionately higher in developing countries; Nigeria remains among the countries heavily affected by cholera and typhoid, largely because of deficiencies in water supply systems, sanitation infrastructure, and hygiene practices that enable disease transmission. The continued occurrence of these diseases highlights the need for effective control strategies and motivates the use of mathematical models to better understand and mitigate their transmission dynamics (Ali et al., 2015).

Several models have been formulated to study cholera and typhoid in isolation. For example, cholera models have incorporated environmental reservoirs, vaccination strategies, and hyper-infectivity (Panja, 2019; Tien & Earn, 2010). Typhoid models, by contrast, have focused on vaccination coverage, treatment strategies, and optimal control approaches (Tilahun, 2019; Tilahun et al., 2017). Sanusi and Yusuf (2023) showed through mathematical analysis that infection quiescence can increase the likelihood of major outbreaks. In addition, Bolaji et al. (2024) examined the spread of monkeypox involving human–rodent interactions, providing valuable insights for epidemic response modeling. Finally, Matsebula and Nyabadza (2022) developed a mathematical model to describe how cholera and typhoid spread.

Previous investigations have largely examined cholera and typhoid separately. The present work integrates both infections into a unified framework, enabling assessment of their combined epidemiological behavior and intervention outcomes. A key contribution of this study lies in capturing the coupled interaction between waterborne (cholera) and directly transmitted (typhoid) infections within a unified modeling framework. This allows the derivation of distinct yet interacting reproduction numbers, providing insight into the independent and joint persistence of the diseases. Furthermore, the model reveals differential sensitivity of cholera and typhoid to intervention strategies and highlights the dominant role of sanitation in controlling environmentally driven transmission.

In addition, the integration of time-dependent optimal control measures enables the assessment of cost-effective intervention strategies in a co-infection setting, which supports the understanding and management of the burden of cholera–typhoid co-infection in endemic regions.

2. MATERIALS AND METHODS

This section presents the formulation of the cholera–typhoid co-infection model and its mathematical analysis. It describes the model structure, assumptions, and governing equations, followed by key analytical properties such as positivity, boundedness, the reproduction number, stability results, and the optimal control framework.

https://doi.org/10.24191/mij.v7i2.12400 ©Authors, 2026

2.1 Model Diagram

Figure 1 depicts the cholera–typhoid co-infection system, highlighting interactions among human population groups and environmental bacterial reservoirs. Individuals progress through susceptible, vaccinated, exposed, infectious, co-infectious, and recovered states, while bacterial levels are increased by infected individuals and reduced through natural decay.

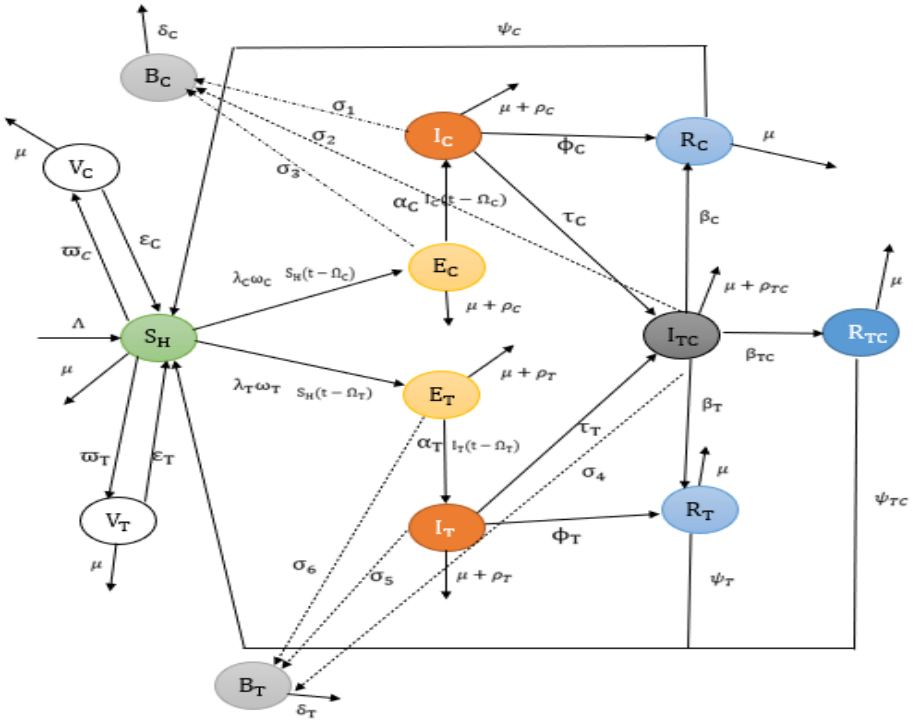


Fig. 1. Schematic diagram of the model

Source: Authors' schematic representation of the proposed cholera–typhoid co-infection model

2.2 Model formulation

A cholera–typhoid co-infection model is formulated by coupling human and environmental bacterial populations. The human population is divided into susceptible S_H, vaccinated V_C, V_T, exposed E_C, E_T, infectious I_C, I_T, co-infected I_{TC}, and recovered compartments R_C, R_T, for both diseases. Individuals are recruited into the susceptible class and may become infected through effective contact with infectious individuals or transition through vaccination, waning immunity, recovery, and natural death. Exposed individuals progress to infection, while infectious individuals may recover, progress to co-infection, or die. Environmental bacteria B_C and B_T increase through shedding from infected classes and decay naturally.

The system of nonlinear differential equations (1) – (13) that describes the behavior of the model results from these interactions:

https://doi.org/10.24191/mij.v7i2.12400 ©Authors, 2026

$$\frac{dS_H}{dt} = \Lambda - (\lambda_C + \lambda_T + \varpi_T + \varpi_C + \mu)S_H + \psi_C R_C + \psi_{TC} R_{TC} + \psi_T R_T + \varepsilon_C V_C + V_T \varepsilon_T \quad (1)$$

$$\frac{dV_C}{dt} = \varpi_C S_H - (\varepsilon_C + \mu)V_C \quad (2)$$

$$\frac{dV_T}{dt} = \varpi_T S_H - (\varepsilon_T + \mu)V_T \quad (3)$$

$$\frac{dE_C}{dt} = \lambda_C S_H - \mathrm{k}_1 E_C \quad (4)$$

$$\frac{dE_T}{dt} = \lambda_T S_H - \mathrm{k}_2 E_T \quad (5)$$

$$\frac{dI_C}{dt} = \alpha_C E_C(t - \Omega_C) - \mathrm{k}_3 I_C \quad (6)$$

$$\frac{dI_T}{dt} = \alpha_T E_T(t - \Omega_T) - \mathrm{k}_4 I_T \quad (7)$$

$$\frac{dI_{TC}}{dt} = \tau_T I_T + \tau_C I_C - \mathrm{k}_5 I_{TC} \quad (8)$$

$$\frac{dR_C}{dt} = \phi_C I_C - (\mu + \psi_C)R_C \quad (9)$$

$$\frac{dR_T}{dt} = \phi_T I_T - (\mu + \psi_T)R_T \quad (10)$$

$$\frac{dR_{TC}}{dt} = \phi_{TC} I_{TC} - (\mu + \psi_{TC})R_{TC} \quad (11)$$

$$\frac{dB_C}{dt} = \beta_C B_C \left(1 - \frac{B_C}{K_C}\right) + \sigma_2 I_C + \sigma_3 E_C + \sigma_1 I_{TC} - \delta_C B_C \quad (12)$$

$$\frac{dB_T}{dt} = \beta_T B_T \left(1 - \frac{B_T}{K_T}\right) + \sigma_5 I_T + \sigma_6 E_T + \sigma_4 I_{TC} - \delta_T B_T \quad (13)$$

where;

$$\mathrm{k}_1 = \alpha_\mathrm{C} + \mu + \rho_\mathrm{C} + \sigma_3\ , \mathrm{k}_2 = \alpha_\mathrm{T} + \mu + \rho_\mathrm{T} + \sigma_6, \mathrm{k}_3 = \phi_\mathrm{C} + \mu + \rho_\mathrm{C} + \tau_\mathrm{C} + \sigma_1,$$
$$\mathrm{k}_4 = \phi_\mathrm{T} + \mu + \rho_\mathrm{T} + \tau_\mathrm{T} + \sigma_5, \mathrm{k}_5 = \phi_\mathrm{TC} + \mu + \rho_\mathrm{CT} + \sigma_2 + \sigma_4. \quad (14)$$

The forces of infection are expressed as follows:

$$\lambda_C = \frac{\phi_{C_1} B_C}{B_C + K_C} + \frac{\mu_{C_2}(I_C + \varrho_C I_{CT})}{N}\ , \lambda_T = \frac{\phi_{T_1} B_T}{B_T + K_T} + \frac{\mu_{T_2}(I_T + \varrho_T I_{CT})}{N},$$
$$\tau_C = \frac{\phi_{C_3} B_C}{B_C + K_C} + \frac{\mu_{C_4}(I_C + \varrho_C I_{CT})}{N},\ \tau_T = \frac{\phi_{T_3} B_T}{B_T + K_T} + \frac{\mu_{T_4}(I_T + \varrho_T I_{CT})}{N}. \quad (15)$$

https://doi.org/10.24191/mij.v7i2.12400 ©Authors, 2026

Table 1. Overview of important model variables

Variables	Description
S_H	Susceptible humans
E_C, E_T	Cholera and typhoid exposed humans, respectively
V_C, V_T	Vaccinated individuals against cholera and typhoid, respectively
I_T, I_C, I_{TC}	Individuals infected with cholera, typhoid fever and cholera-typhoid infected
R_C, R_T, R_{TC}	Individuals recovered from cholera, Typhoid and Cholera-typhoid infections
B_C, B_T	Cholerae Typhi concentration and Salmonella bacteria concentration

Source: Authors' definitions of the variables in the cholera–typhoid co-infection model

2.3 Positivity of Solution

For epidemiological validity, it is necessary to establish for all state variables remain non-negative at all future times whenever the initial conditions are non-negative.

Proof

Consider the susceptible human population

$$\frac{\mathrm{dS_H}}{\mathrm{dt}} = \Lambda - (\lambda_\mathrm{C} + \lambda_\mathrm{T} + \varpi_T + \varpi_C + \mu)\mathrm{S_H} + \psi_\mathrm{C}\mathrm{R_C} + \psi_\mathrm{TC}\mathrm{R_{TC}} + \psi_\mathrm{T}\mathrm{R_T} + \varepsilon_C V_C + V_T\varepsilon_T. \tag{16}$$

Separating variables and integrating yields:

$$\begin{aligned} &\int \tfrac{1}{\mathrm{S_H}}\mathrm{dS_H} = -\int(\lambda_\mathrm{C} + \lambda_\mathrm{T} + \varpi_T + \varpi_C + \mu)\,dt, \\ &\ln \mathrm{S_H} = -A(t) + \mathrm{c_1} \end{aligned} \tag{17}$$

where

$A(t) = -\int_0^t(\lambda_\mathrm{C} + \lambda_\mathrm{T} + \varpi_T + \varpi_C + \mu)dt$ and $\mathrm{c_1}$ is the constant of integration. Exponentiating gives

$$\mathrm{S_H} = De^{-A(t)},\ D = e^{\mathrm{c_1}} \geq 0 \text{ at } t = 0, S_H > 0. \tag{18}$$

Hence $S_H(t) \geq 0\ \forall\ t \geq 0$ provided $S_H(0) \geq 0$.

Similarly, for the vaccinated compartments:

$$\begin{aligned} &\tfrac{\mathrm{dV_C}}{\mathrm{dt}} = \varpi_C\mathrm{S_H} - (\varepsilon_\mathrm{C} + \mu)\mathrm{V_C}, \\ &\tfrac{\mathrm{DV_T}}{\mathrm{dt}} = \varpi_T\mathrm{S_H} - (\varepsilon_T + \mu)V_T. \end{aligned} \tag{19}$$

Integrating yields

$$\mathrm{V_C} = Ge^{-F(t)}\ \mathrm{V_T} = Je^{-L(t)},\ \mathrm{G, J} \geq 0. \tag{20}$$

So $\mathrm{V_C}(t), \mathrm{V_T}(t) \geq 0$ for all $t \geq 0$.
Applying the same procedure to the exposed, infected, and recovered compartments gives:

$$\mathrm{E_C}(t), \mathrm{E_T}(t), \mathrm{I_C}(t), \mathrm{I_T}(t), \mathrm{I_{TC}}, \mathrm{R_C}(t), \mathrm{R_T}(t), \mathrm{R_{TC}}(t) \geq 0\ \forall\ t \geq 0. \tag{21}$$

Also, for the bacterial reservoirs

 ©Authors, 2026

$$\mathrm{B_C}(t), \mathrm{B_T}(t) \geq 0 \; \forall \; t \geq 0. \tag{22}$$

Therefore, every state variable of the cholera–typhoid co-infection model remains non-negative for all time, provided the initial conditions are non-negative. Hence, the model's feasible region is positively invariant.

2.4 Reproduction Number R_0

The basic reproduction number, denoted by R_0, represents the average number of secondary infections generated by a single infectious individual introduced into an entirely susceptible population. It serves as a threshold quantity that determines whether disease invasion can occur. If $\mathrm{R_0} < 1$, the introduction of cholera and typhoid infections into the population will not lead to sustained transmission, and the co-infection will eventually be eliminated. Conversely, if $\mathrm{R_0} > 1$, both cholera and typhoid infections will persist in the population, leading to endemicity.

Applying the Van den Driessche and Watmough (2002) approach to Eqs. (4) – (8) and (12) – (13), which govern infection dynamics, yields the following:

In the absence of disease at equilibrium,

$$S_H^* = \frac{\Lambda}{\mu}, E_C = E_T = I_C = I_T = I_{TC} = B_C = B_T = 0. \tag{23}$$

Linearization about the disease-free equilibrium produces the matrices (F) and (V), where (F) captures the appearance of new infections and (V) describes all other transfers among infected compartments,

$$F = \begin{pmatrix} 0 & 0 & \frac{\mu_{C_2} S_H^*}{N} & 0 & \frac{\varrho_C \mu_{C_2} S_H^*}{N} & \frac{\phi_{C_1} S_H^*}{K_C} & 0 \\ 0 & 0 & 0 & \frac{\mu_{T_2} S_H^*}{N} & \frac{\varrho_T \mu_{T_2} S_H^*}{N} & 0 & \frac{\phi_{T_1} S_H^*}{K_T} \\ 0 & 0 & 0 & 0 & 0 & 0 & 0 \\ 0 & 0 & 0 & 0 & 0 & 0 & 0 \\ 0 & 0 & \tau_C & \tau_T & 0 & 0 & 0 \\ 0 & 0 & 0 & 0 & 0 & 0 & 0 \\ 0 & 0 & 0 & 0 & 0 & 0 & 0 \end{pmatrix}, V = \begin{pmatrix} k_1 & 0 & 0 & 0 & 0 & 0 & 0 \\ 0 & k_2 & 0 & 0 & 0 & 0 & 0 \\ -\alpha_c & 0 & k_3 & 0 & 0 & 0 & 0 \\ 0 & -\alpha_T & 0 & k_4 & 0 & 0 & 0 \\ 0 & 0 & 0 & 0 & k_5 & 0 & 0 \\ -\sigma_3 & 0 & -\sigma_2 & 0 & -\sigma_1 & \delta_c & 0 \\ 0 & -\sigma_6 & 0 & -\sigma_5 & -\sigma_4 & 0 & \delta_T \end{pmatrix}. \tag{24}$$

Then the general matrix becomes:

$$FV^{-1} = \begin{pmatrix} 0 & 0 & \frac{\mu_{C_2} S_H^*}{N k_3} & 0 & \frac{\varrho_C \mu_{C_2} S_H^*}{N k_5} & \frac{\phi_{C_1} S_H^*}{K_C \delta_C} & 0 \\ 0 & 0 & 0 & \frac{\mu_{T_2} S_H^*}{N k_4} & \frac{\varrho_T \mu_{T_2} S_H^*}{N k_5} & 0 & \frac{\phi_{T_1} S_H^*}{K_T \delta_T} \\ 0 & 0 & 0 & 0 & 0 & 0 & 0 \\ 0 & 0 & 0 & 0 & 0 & 0 & 0 \\ 0 & 0 & \frac{\tau_C}{k_3} & \frac{\tau_T}{k_4} & 0 & 0 & 0 \\ 0 & 0 & 0 & 0 & 0 & 0 & 0 \\ 0 & 0 & 0 & 0 & 0 & 0 & 0 \end{pmatrix}. \tag{25}$$

The dominant eigenvalue of the matrix (FV^{-1}) yields the effective reproduction number for the coupled cholera–typhoid transmission process. The eigenvalues representing the two reproduction numbers are expressed as:

$$R_c = \frac{\mu_{C_2} S_H}{N k_3} + \frac{\phi_{C_1} S_H}{K_C \delta_C} + \frac{\varrho_C \mu_{C_2} S_H}{N k_5}, R_T = \frac{\mu_{T_2} S_H}{N k_4} + \frac{\phi_{T_1} S_H}{K_T \delta_T} + \frac{\varrho_T \mu_{T_2} S_H}{N k_5}. \tag{26}$$

So that $R_0 = \max\{R_C, R_T\}$.

2.5 Sensitivity Analysis of the Basic Reproduction Number

To determine the epidemiological parameters that most strongly influence cholera–typhoid transmission, a sensitivity analysis of the basic reproduction number is performed. The normalized forward sensitivity index of R_0 with respect to a parameter P is defined as:

$$\Upsilon_P^{R_0} = \frac{\partial R_0}{\partial P} \times \frac{P}{R_0} \tag{27}$$

where $\Upsilon_P^{R_0}$ denotes the sensitivity index of the basic reproduction number with respect to parameter P. This measure quantifies the relative change in R_0 resulting from a relative change in the parameter. Parameters with positive sensitivity values increase disease transmission as their magnitudes rise, whereas those with negative values contribute to lowering transmission and enhancing disease control.

2.6 Global Stability of Disease-Free Equilibrium (DFE)

Global asymptotic stability implies that, irrespective of the initial conditions, system trajectories eventually approach and remain at the equilibrium state. Various techniques have been developed to establish the global stability of the disease-free equilibrium (DFE), including the approaches proposed by Perasso (2018) and Van den Driessche (2017) as well as the Lyapunov function method. In this work, we employ the Lyapunov function approach.

Theorem 1

The disease-free equilibrium (DFE) of the system defined in Eqs. (1) – (13) is globally asymptotically stable.

Proof

We consider the following Lyapunov function:

$$\begin{aligned} \mathrm{V(t)} = {} & (S_H - {S_H}^* \ln S_H) + (V_C - {V_C}^* \ln V_C) + (V_T - {V_T}^* \ln V_T) + E_C + E_T + I_C + I_T \\ & + I_{TC} + R_C + R_T + R_{TC} + B_C + B_T. \end{aligned} \tag{28}$$

Differentiating with respect to time, we have

$$\begin{aligned} \dot{\mathrm{V}}(\mathrm{t}) = {} & \dot{S}_H \left(1 - \frac{{S^*}_H}{S_H}\right) + \dot{V}_C \left(1 - \frac{{V_C}^*}{V_C}\right) + \dot{V}_T \left(1 - \frac{{V_T}^*}{V_T}\right) + \dot{E}_C + \dot{E}_T + \dot{I}_C + \dot{I}_T + \dot{I_{TC}} \\ & + \dot{R}_C + \dot{R}_T + \dot{R}_{TC} + \dot{B}_C + \dot{B}_T. \end{aligned} \tag{29}$$

Substituting the system dynamics, simplifying, and collecting terms yields

$$\begin{aligned} \dot{\mathrm{V}}(\mathrm{t}) = {} & \Lambda \left(1 - \frac{{S^*}_H}{S_H}\right) + k_1 {S^*}_H \left(1 - \frac{S_H}{{S^*}_H}\right) + k_2 {V^*}_C \left(1 - \frac{V_C}{{V^*}_C}\right) + k_3 {V^*}_T \left(1 - \frac{V_T}{{V^*}_T}\right) \\ & - \delta(R_C + R_T + R_{TC}). \end{aligned} \tag{30}$$

From the above, it follows that

$$\begin{aligned} \dot{\mathrm{V}}(\mathrm{t}) \leq {} & \Lambda \left(1 - \frac{{S^*}_H}{S_H}\right) + k_1 {S^*}_H \left(1 - \frac{S_H}{{S^*}_H}\right) + k_2 {V^*}_C \left(1 - \frac{V_C}{{V^*}_C}\right) + k_3 {V^*}_T \left(1 - \frac{V_T}{{V^*}_T}\right) \\ & - \delta(R_C + R_T + R_{TC}). \end{aligned} \tag{31}$$

Clearly , $\dot{\mathrm{V}}(\mathrm{t}) \leq 0$ only when $R_C + R_T + R_{TC} = 0$. Therefore, the largest invariant set in Ω is the singleton set ε_0. By LaSalle's invariance principle, the DFE ε_0 is globally asymptotically stable on Ω whenever $R_C < 0$.

https://doi.org/10.24191/mij.v7i2.12400 ©Authors, 2026

2.7 Global Stability of Endemic Equilibrium

The global stability of the endemic equilibrium indicates that, when the reproduction number exceeds unity, the infection persists and solutions converge to that equilibrium.

Theorem 2

If $R_0 > 1$, then the unique endemic equilibrium E^{**} is globally asymptotically stable on Ω such that $\mathrm{E}_C = \mathrm{E}_T = \mathrm{I}_C = \mathrm{I}_T = \mathrm{I}_{TC} = 0$.

Proof

Consider the Lyapunov function $l = \sum_{i=1}^{13} \mathrm{a}_i(\mathrm{x}_i - x_i^* \ln x_i)$ where $\mathrm{a}_i > 0$ are suitably chosen positive constants, x_i is the population of i^{th}compartment, and x_i^* is the equilibrium point, which is an endemic point. The Lyapunov function for the full model system is

$$\begin{aligned} l = {} & a_1(S_H - S_H^* \ln S_H) + a_2(V_C - V_C^* \ln V_C) + a_3(V_T - V_T^* \ln V_T) + a_4(E_C - E_C^* \ln E_C) \\ & + a_5(E_T - E_T^* \ln E_T) + a_6(I_C - I_C^* \ln I_C) + a_7(I_T - I_T^* \ln I_T) + a_8(I_{TC} - I_{TC}^* \ln I_{TC}) \\ & + a_9(R_C - R_C^* \ln R_C) + a_{10}(R_T - R_T^* \ln R_T) + a_{11}(R_{TC} - R_{TC}^* \ln R_{CT}) \\ & + a_{12}(B_C - B_C^* \ln B_C) + a_{13}(B_T - B_T^* \ln B_T). \end{aligned} \tag{32}$$

For the cholera compartment, we define

$$\begin{aligned} l_C = {} & a_1(S_H - S_H^* \ln S_H) + a_2(V_C - V_C^* \ln V_C) + a_3(E_C - E_C^* \ln E_C) \\ & + a_5(I_C - I_C^* \ln I_C) + a_6(R_C - R_C^* \ln R_C) + a_7(B_C - B_C^* \ln B_C). \end{aligned} \tag{33}$$

Differentiating with respect to time yields

$$\frac{dl_C}{dt} = \sum_i a_i \left(1 - \frac{x_i^*}{x_i}\right) \frac{dx_i}{dt}. \tag{34}$$

At the endemic equilibrium point E^{**}, it simplifies to

$$\frac{dl_C}{dt} = -a_1(\varpi_C + \mu)\left(1 - \frac{{S^*}_H}{S_H}\right)^2 - a_1\lambda_C\left(1 - \frac{{S^*}_H}{S_H}\right)^2 + Z_C(S_H, V_C, E_C, I_C, R_C, B_C) \tag{35}$$

where Z_C is a non-negative function.

Similarly, for the typhoid compartments, we define

$$\begin{aligned} l_T = {} & a_7(S_H - S_H^* \ln S_H) + a_8(V_T - V_T^* \ln V_T) + a_9(E_T - E_T^* \ln E_T) \\ & + a_{10}(I_T - I_T^* \ln I_T) + a_{11}(R_T - R_T^* \ln R_T) + a_{12}(B_T - B_T^* \ln B_T) \end{aligned} \tag{36}$$

with the time derivative

$$\frac{dl_T}{dt} = -a_7(\varpi_T + \mu)\left(1 - \frac{{S^*}_H}{S_H}\right)^2 - a_7\lambda_T\left(1 - \frac{{S^*}_H}{S_H}\right)^2 + Z_T(S_H, V_T, E_T, I_T, R_T, B_T) \tag{37}$$

where $Z_T \leq 0$ by LaSalle's invariance principle. Since $Z_C, Z_T \leq 0$ for all positive compartment values, it follows that $\frac{dl}{dt} \leq 0$ with equality holding only at the endemic equilibrium,

$$S_H = \mathrm{S}_H^*, V_C = \mathrm{V}_C^*, V_T = \mathrm{V}_T^*, E_T = \mathrm{E}_T^*, \ldots., B_T = \mathrm{B}_T^*. \tag{38}$$

Therefore, E^{**} is globally asymptotically stable.

https://doi.org/10.24191/mij.v7i2.12400 ©Authors, 2026

3. OPTIMAL CONTROL OF THE CHOLERA–TYPHOID CO-INFECTION MODEL

Optimal control theory enables us to derive time-dependent intervention functions (e.g., vaccination, treatment, and sanitation) that minimize a composite cost functional reflecting both disease burden and intervention costs (Adu et al., 2026).

Let the state vector be

$$x(t) = S_H, V_C, V_T, E_C, E_T, I_C, I_T, I_{TC}, R_C, R_T, R_{TC}, B_C, B_T \tag{39}$$

and define the control functions $U_1(t), U_2(t)$ and $U_3(t)$ representing vaccination, treatment, and sanitation efforts, respectively. Under these controls, the susceptible and infected classes are modified. For example, the susceptible population evolves as infection pressure decreases through vaccination, while the infected compartment is further reduced through treatment. Environmental reservoirs are likewise lowered through sanitation control.

The objective functional is formulated as:

$$J(U_1, U_2, U_3) = \int_0^T \left[A_1 I_C(t) + A_2 I_T(t) + A_3 I_{TC}(t) + \frac{1}{2}(B_1 U_1^2 + B_2 U_2^2 + B_3 U_3^2)\right] dt \tag{40}$$

where $A_i \geq 0, B_i > 0$ balance disease burden and intervention costs. The controls satisfy $0 \leq U_i(t) \leq U_i{}^{max}, i = 1,2,3$.

Using Pontryagin's Maximum Principle, the Hamiltonian is constructed and adjoint variables $\lambda_i(t)$ are introduced. The adjoint system satisfies:

$$\frac{d\lambda_i}{dt} = -\frac{\delta H}{\delta x_i}, \lambda_i(T) = 0 \ (i = 1, \ldots, 13). \tag{41}$$

Optimal controls are obtained from the first-order conditions:

$$\begin{aligned} U_1^*(t) &= \min\left(U_1^{max}, max\left(0, \frac{\lambda_1 S_H}{B_1}\right)\right), \\ U_2^*(t) &= \min\left(U_2^{max}, max\left(0, \frac{\lambda_6 I_C + \lambda_7 I_T + \lambda_8 I_{TC}}{B_2}\right)\right), \\ U_3^*(t) &= \min\left(U_2^{max}, max\left(0, \frac{\lambda_2 V_C + \lambda_3 V_T}{B_3}\right)\right). \end{aligned} \tag{42}$$

The resulting optimality system is solved numerically using the forward–backward sweep method (Armengou-Riera et al., 2026), yielding optimal time profiles that reduce infection levels while controlling intervention costs.

Finally, the economic evaluation is performed using the Average Cost-Effectiveness Ratio (ACER):

$$ACER = \frac{C_{\mathrm{i}}}{E_{\mathrm{i}}} \tag{43}$$

where (C_i) represents the total cost associated with control strategy (i), and (E_i) denotes the corresponding epidemiological effectiveness measured as infections averted.

https://doi.org/10.24191/mij.v7i2.12400 ©Authors, 2026

4. RESULTS AND DISCUSSION

This section presents numerical simulations, model validation, and interpretation of the epidemiological behavior of the system under different intervention scenarios.

4.1 Analysis of the Model

The epidemiological data are derived from publicly available epidemiological reports and published sources were used to simulate the formulated cholera–typhoid co-infection model under two distinct conditions: the absence of health interventions ($H = 0$) and the implementation of moderate interventions ($H = 0.25$) here, H represents the intensity of health measures such as sanitation, treatment, and vaccination.

Simulation results were displayed graphically, and the two control scenarios were compared to examine the effectiveness of intervention measures in reducing disease spread. Model calibration and validation were carried out using reported cholera and typhoid incidence data obtained from the Nigeria Centre for Disease Control and the World Health Organization.

Theorem 1 establishes that when the reproduction number is below unity, the disease-free equilibrium is globally asymptotically stable. Numerical results support this finding, as effective interventions reduce transmission and disease prevalence. Model parameters were estimated through a nonlinear least-squares optimization that minimized the difference between simulated and observed data. Numerical simulations were implemented in MATLAB using the dde23 solver, and the fitted results showed strong agreement with epidemiological observations, as illustrated in Figure 2 for cholera and typhoid infections.

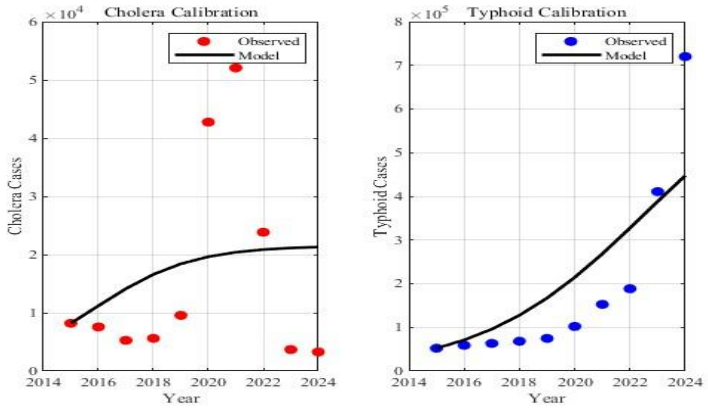


Fig. 2. Comparison between the (left) model predictions and (right) observed data for cholera and typhoid infections

Source: Authors' model predictions and epidemiological data attributed to the Nigeria Centre for Disease Control (NCDC) and the World Health Organization (WHO)

The numerical results are interpreted using the epidemiological compartments defined in Table 1, including the susceptible, vaccinated, exposed, infected, recovered, and environmental bacterial classes. These variables provide the basis for assessing disease progression and the effects of vaccination, treatment, and sanitation interventions.

https://doi.org/10.24191/mij.v7i2.12400 ©Authors, 2026

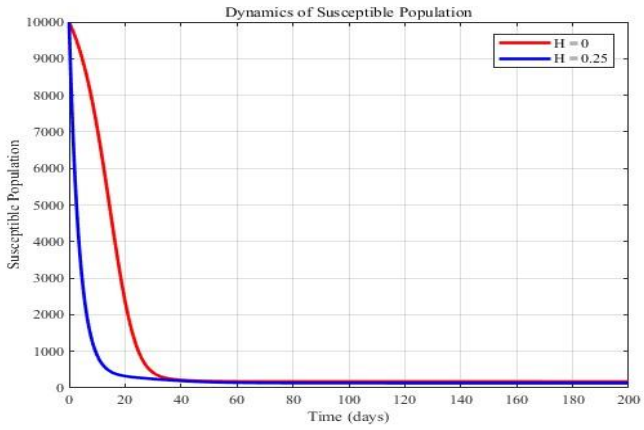


Fig. 3. Temporal dynamics of the susceptible population under no intervention (H = 0) and moderate intervention (H = 0.25)

Source: Authors' numerical simulations of the susceptible population

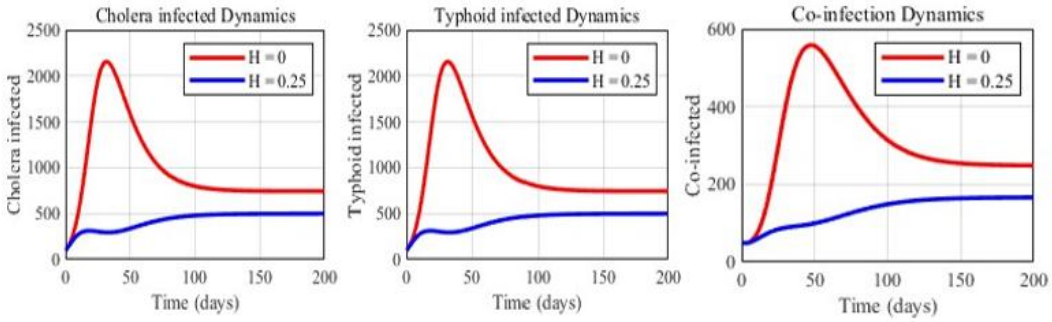


Fig. 4. Temporal dynamics of (left) cholera-infected, (middle) typhoid-infected, and (right) co-infected populations under no intervention (H = 0) and moderate intervention (H = 0.25)

Source: Authors' numerical simulations of cholera-infected, typhoid-infected, and co-infected populations

https://doi.org/10.24191/mij.v7i2.12400 ©Authors, 2026

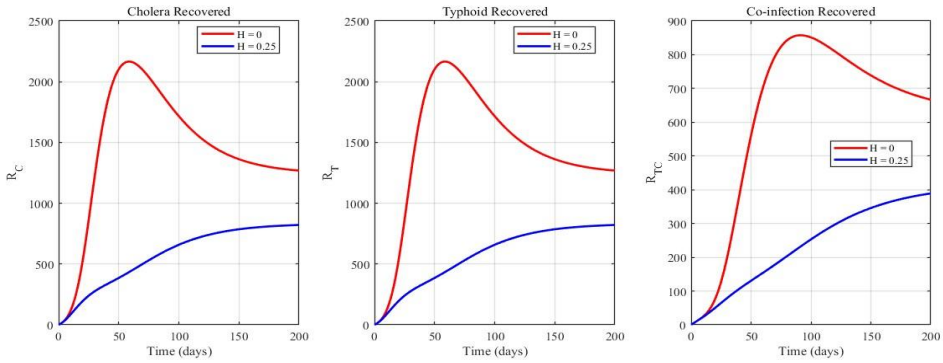


Fig. 5. Temporal dynamics of (left) cholera-recovered, (middle) typhoid-recovered, and (right) co-infection-recovered populations under no intervention (H = 0) and moderate intervention (H = 0.25)

Source: Authors' numerical simulations of cholera-recovered, typhoid-recovered, and co-infection-recovered populations

The dynamical analysis in Figures 3–5 showed that, without intervention, the susceptible population declined rapidly due to high infection pressure. In contrast, intervention measures significantly slowed this depletion and maintained a higher long-term susceptible population. Cholera dynamics exhibited a pronounced outbreak peak without intervention because of strong environmental transmission, whereas moderate intervention substantially reduced both peak prevalence and outbreak duration.

Typhoid dynamics showed weaker sensitivity to intervention intensity, suggesting a stronger dependence on direct human-to-human transmission than on environmental contamination. Co-infection dynamics indicated that simultaneous infection greatly increased disease burden, but integrated control measures effectively reduced both the prevalence and persistence of co-infected individuals. Theorem 2 shows that when the reproduction number exceeds unity, the infection persists and solutions converge to the endemic equilibrium. Numerical results support this finding, and vaccination, treatment, and sanitation reduce the disease burden.

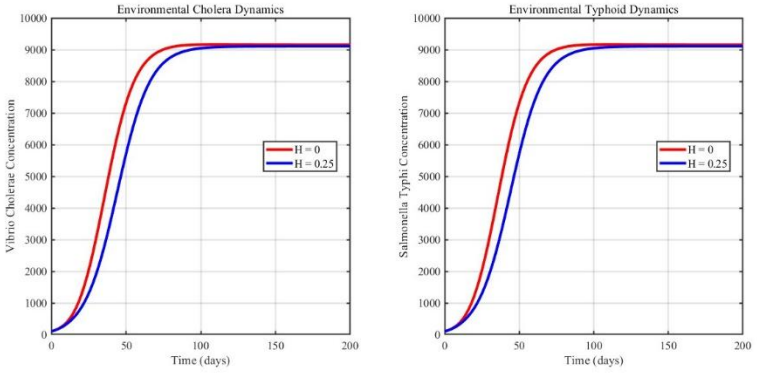


Fig. 6. Temporal dynamics of (left) Vibrio cholerae and (right) Salmonella Typhi concentration under no intervention (H = 0) and moderate intervention (H = 0.25)

Source: Authors' numerical simulations of environmental Vibrio cholerae and Salmonella Typhi concentrations

https://doi.org/10.24191/mij.v7i2.12400 ©Authors, 2026

Environmental reservoir simulations shown in Figure 6 demonstrated that *Vibrio cholerae* concentrations rose rapidly during the early epidemic phase due to bacterial shedding from infected individuals. Intervention measures significantly reduced environmental bacterial load through improved sanitation and lower transmission. A similar but less pronounced pattern was observed for *Salmonella Typhi*, confirming that environmental sanitation plays a more important role in cholera control than in typhoid transmission.

The tornado diagram in Figure 7 shows the normalized sensitivity of the basic reproduction number, R_0, to key parameters in the delayed cholera–typhoid co-infection model. Positive sensitivity indicates that increasing a parameter increases R_0, while negative sensitivity indicates a reduction in R_0, with larger absolute values representing stronger influence. The results show that ϕ_{C_1} and ϕ_{T_1}, representing environmental transmission contributions, have strong positive effects on R_0, highlighting the importance of bacterial reservoirs in disease transmission. Similarly, μ_{C_2} and μ_{T_2} exhibit positive sensitivity, indicating that increased human-to-human transmission enhances the reproduction potential of cholera and typhoid, respectively, while ϱ_C and ϱ_T also contribute positively, reflecting the role of co-infection in increasing transmission potential. In contrast, δ_C and δ_T have negative sensitivity. Because these parameters occur in the denominators of the environmental transmission terms, increasing bacterial removal or decay reduces the contribution of the environmental reservoirs to transmission and consequently lowers the reproduction number. The parameters K_C and K_T also show negative sensitivity, indicating that increases in the corresponding environmental scaling or half-saturation quantities reduce the environmental contribution to R_C and R_T.

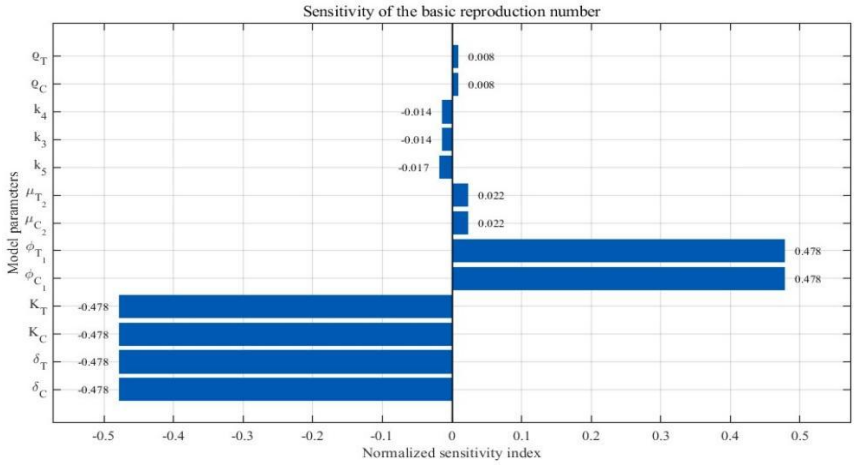


Fig. 7. The tornado diagram illustrates the relative influence of epidemiological parameters on the basic reproduction number R_0

Source: Authors' sensitivity analysis of the model's basic reproduction number

4.2 Cost-Effectiveness Results

The comparative analysis of cholera and typhoid control strategies is presented in Table 2, where four interventions, namely vaccination, sanitation, treatment, and combined control, are evaluated based on infections averted and associated costs.

https://doi.org/10.24191/mij.v7i2.12400 ©Authors, 2026

Table 2. Comparative cost-effectiveness analysis of cholera and typhoid control strategies showing the number of infections averted and associated costs for vaccination, sanitation, treatment, and combined interventions, used to evaluate the economic efficiency.

Control strategies	No. of cholera infections averted	Cost	No. of typhoid infections averted	Cost
Vaccination	15132	945678.10	17133	915222.80
Sanitation	42822	623151.20	32820	515896.20
Treatment	23839	1700082.55	25830	1113459.8
Combined	81793	3268911.85	75783	2544572.8

Source: Authors' model-based calculations of infections averted and intervention costs

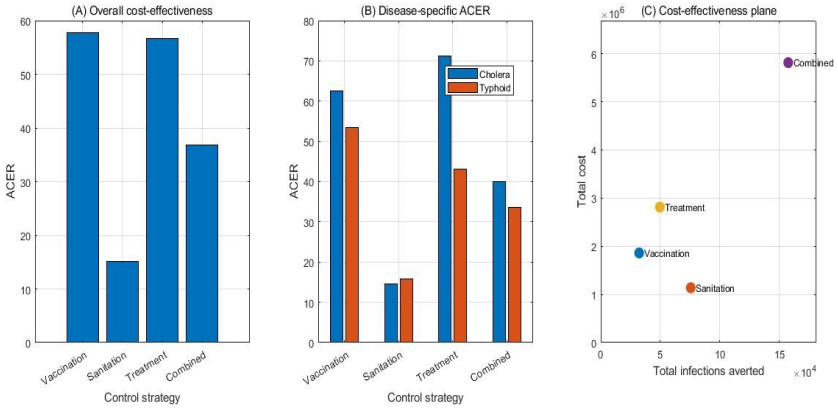


Fig. 8. Cost-effectiveness analysis of control strategies using ACER; (left) overall ACER shows sanitation as the most cost-effective; (middle) disease-specific ACER confirms sanitation's efficiency for both cholera and typhoid; (right) the cost-effectiveness plane shows the combined strategy has the highest impact but also the highest cost.

Source: Authors' cost-effectiveness calculations

Figure 8 presents the cost-effectiveness analysis of vaccination, sanitation, treatment, and combined strategies using ACER. Figure 8 (left) shows overall ACER values, with sanitation the most cost-effective and the combined strategy the least efficient. Figure 8 (middle) presents disease-specific ACER results for cholera and typhoid, confirming sanitation as the most efficient intervention in both cases, while vaccination and treatment show moderate performance. Figure 8 (right) illustrates the cost-effectiveness plane, where the combined strategy achieves the greatest impact but at the highest cost. Overall, Figure 8 indicates that sanitation provides the best balance between cost and effectiveness. These findings suggest that the optimal allocation of limited public health resources should prioritize sanitation interventions while complementing them with targeted treatment and vaccination efforts.

5. CONCLUSION

A deterministic nonlinear model for cholera–typhoid co-infection was developed to incorporate environmental transmission, latency, vaccination, treatment, recovery, and bacterial dynamics. The model was verified to be well-posed by establishing the non-negativity and boundedness of its solutions. Furthermore, the basic reproduction number R_0 emerged as the principal threshold indicator: disease extinction occurs when $R_0 < 1$, whereas endemic persistence is expected when $R_0 > 1$.

https://doi.org/10.24191/mij.v7i2.12400 ©Authors, 2026

The global stability analysis confirmed the asymptotic convergence of solutions to the disease-free and endemic equilibrium points when the associated threshold conditions are met. Sensitivity analysis showed that cholera transmission is mainly driven by environmental contamination, whereas typhoid spread is more affected by direct human contact.

Optimal control results revealed that vaccination, treatment, and sanitation measures significantly reduced the prevalence of infection and bacterial concentrations. Cost-effectiveness analysis indicated that sanitation is the most efficient strategy for cholera control, whereas combined interventions provide the greatest reduction in co-infection burden. Overall, integrated control strategies are essential for the effective management of cholera–typhoid co-infection in endemic settings.

The findings indicate that environmental transmission and control interventions play important roles in cholera–typhoid dynamics. However, the environmental component is represented by simplified bacterial reservoir dynamics and does not include climatic factors or stochastic outbreak variations, which may influence the observed transmission patterns.

Future studies could incorporate climatic and spatial factors, stochastic transmission, and more detailed epidemiological data. Adaptive control strategies may also be investigated to improve the effectiveness and sustainability of interventions.

6. ACKNOWLEDGMENTS/FUNDING

The authors appreciate the management of Federal University Dutsin-Ma for their support and for the knowledge gained from earlier research, which guided the parameter values and the modeling framework applied in this study.

7. CONFLICT OF INTEREST STATEMENT

The authors report no conflict of interest regarding this research.

8. AUTHORS' CONTRIBUTIONS

Chinenye Nworah conceptualized the study, developed the methodology, conducted the analysis, and prepared the original draft. Abdu Masanawa Sagir carried out the investigation, supervised the work, and reviewed and edited the manuscript. Joel M. Orverem contributed to the software implementation, while validation was performed by Yusuf. A Bichi.

9. DECLARATION OF GENERATIVE AI IN THE WRITING PROCESS

During the preparation of this manuscript, the authors reviewed, verified, and edited all AI-assisted content and take full responsibility for the accuracy, originality, and integrity of the final manuscript. Generative AI was not used to generate or replace the scientific analysis, mathematical derivations, numerical results, or conclusions of the study.

 ©Authors, 2026

10. DATA AVAILABILITY/SUPPLEMENTARY MATERIALS

The data used in this study are derived from publicly available epidemiological reports and published sources:

i. https://ncdc.gov.ng/diseases/sitreps/?cat=7&name=an%2bupdate%2bof%2bcholera%2boutbreak%2bin%2bnigeria

ii. https://immunizationdata.who.int/global?topic=&location=

11. ETHICS STATEMENT

This study involved mathematical modeling and analysis of publicly available epidemiological data. No human participants, personal data, human biological samples, or animal subjects were involved. Therefore, ethical approval and informed consent were not required.

REFERENCES

Adu, I. K., Asamoah, J. K. K., Wireko, F. A., Afosaa, V., & Foriwaa, K. A. (2026). Mathematical modelling of absenteeism with optimal control analysis. *Quality & Quantity, 60*(2), 6899–6938. https://doi.org/10.1007/s11135-025-02566-0

Akinyemi, K. O., Ajoseh, S. O., & Fakorede, C. O. (2021). A systemic review of literatures on human *Salmonella enterica* serovars in Nigeria (1999–2018). *The Journal of Infection in Developing Countries, 15*(9), 1222–1235. https://doi.org/10.3855/jidc.12186

Ali, M., Nelson, A. R., Lopez, A. L., & Sack, D. A. (2015). Updated global burden of cholera in endemic countries. *PLOS Neglected Tropical Diseases*, *9*(6), e0003832. https://doi.org/10.1371/journal.pntd.0003832

Armengou-Riera, N., Rabiei, N., Bijalwan, A., Rodríguez-Ferran, A., & Muñoz, J. J. (2026). On the convergence of conjugate gradient and GMRES algorithms in the forward backward sweep method for optimal control. *Optimal Control Applications and Methods, 47*(2), 498–510. https://doi.org/10.1002/oca.70072

Azman, A. S., Rudolph, K. E., Cummings, D. A. T., & Lessler, J. (2013). The incubation period of cholera: A systematic review. *Journal of Infection*, *66*(5), 432–438. https://doi.org/10.1016/j.jinf.2012.11.013

Bolaji, L. K., Sagir, A. M., & Balogun, F. (2024). Mathematical transmission dynamics and intervention strategies for monkeypox: A model-based approach including human-rodent interactions. *UMYU Scientifica*, *3*(4), 288–299. https://doi.org/10.56919/usci.2434.023

Gouda, Z. A. (2024). Enteric fever (typhoid and paratyphoid fever). *SHIFAA*, *2024*, 56–62. https://doi.org/10.70470/SHIFAA/2024/007

Matsebula, L., & Nyabadza, F. (2022). Mathematical analysis of cholera typhoid co-infection transmission dynamics. *Frontiers in Applied Mathematics and Statistics*, *8*, 892098. https://doi.org/10.3389/fams.2022.892098

Panja, P. (2019). Optimal control analysis of a cholera epidemic model. *Biophysical Reviews and Letters*, *14*(01), 27–48. https://doi.org/10.1142/S1793048019500024

 ©Authors, 2026

Perasso, A. (2018). An introduction to the basic reproduction number in mathematical epidemiology. *ESAIM: Proceedings and Surveys*, *62*, 123–138. https://doi.org/10.1051/proc/201862123

Sanusi, U., & Yusuf, T. A. (2023). Quiescence raises the risk of major pandemic outbreaks: Insights from mathematical modelling. *UMYU Scientifica*, *2*(3), 15–19. https://doi.org/10.56919/usci.2323.003

Sibaroni, Y., Prasetiyowati, S. S., & Sudrajat, I. B. (2020). Determination of dengue hemorrhagic fever disease factors using neural network and genetic algorithms. *Mathematical Sciences and Informatics Journal*, *1*(2), 77–86. https://doi.org/10.24191/mij.v1i2.14196

Stanaway, J. D., Reiner, R. C., Blacker, B. F., Goldberg, E. M., Khalil, I. A., Troeger, C. E., Andrews, J. R., Bhutta, Z. A., Crump, J. A., Im, J., Marks, F., Mintz, E., Park, S. E., Zaidi, A. K. M., Abebe, Z., Abejie, A. N., Adedeji, I. A., Ali, B. A., Amare, A. T., … Hay, S. I. (2019). The global burden of typhoid and paratyphoid fevers: A systematic analysis for the Global Burden of Disease Study 2017. *The Lancet Infectious Diseases*, *19*(4), 369–381. https://doi.org/10.1016/S1473-3099(18)30685-6

Tien, J. H., & Earn, D. J. D. (2010). Multiple transmission pathways and disease dynamics in a waterborne pathogen model. *Bulletin of Mathematical Biology*, *72*(6), 1506–1533. https://doi.org/10.1007/s11538-010-9507-6

Tilahun, G. T. (2019). Modeling co-dynamics of pneumonia and meningitis diseases. *Advances in Difference Equations*, *2019*, Article 149. https://doi.org/10.1186/s13662-019-2087-3

Tilahun, G. T., Makinde, O. D., & Malonza, D. (2017). Modelling and optimal control of typhoid fever disease with cost-effective strategies. *Computational and Mathematical Methods in Medicine, 2017*, Article 2324518. https://doi.org/10.1155/2017/2324518

Van den Driessche, P. (2017). Reproduction numbers of infectious disease models. *Infectious Disease Modelling, 2*(3), 288–303. https://doi.org/10.1016/j.idm.2017.06.002

Van den Driessche, P., & Watmough, J. (2002). Reproduction numbers and sub-threshold endemic equilibria for compartmental models of disease transmission. *Mathematical Biosciences, 180*(1–2), 29–48. https://doi.org/10.1016/S0025-5564(02)00108-6



© 2026 by the authors. Submitted for possible open access publication under the terms and conditions of the Creative Commons Attribution (CC BY-NC-ND) license (http://creativecommons.org/licenses/by/4.0/).